Biological Psychiatry

Archival Report

Gray Matter Neuritic Microstructure Deficits in Schizophrenia and Bipolar Disorder

Arash Nazeri, Benoit H. Mulsant, Tarek K. Rajji, Melissa L. Levesque, Jon Pipitone, Laura Stefanik, Saba Shahab, Tina Roostaei, Anne L. Wheeler, Sofia Chavez, and Aristotle N. Voineskos

ABSTRACT

BACKGROUND: Postmortem studies have demonstrated considerable dendritic pathologies among persons with schizophrenia and to some extent among those with bipolar I disorder. Modeling gray matter (GM) microstructural properties is now possible with a recently proposed diffusion-weighted magnetic resonance imaging modeling technique: neurite orientation dispersion and density imaging. This technique may bridge the gap between neuroimaging and histopathological findings.

METHODS: We performed an extended series of multishell diffusion-weighted imaging and other structural imaging series using 3T magnetic resonance imaging. Participants scanned included individuals with schizophrenia (n = 36), bipolar I disorder (n = 29), and healthy controls (n = 35). GM-based spatial statistics was used to compare neurite orientation dispersion and density imaging–driven microstructural measures (orientation dispersion index and neurite density index [NDI]) among groups and to assess their relationship with neurocognitive performance. We also investigated the accuracy of these measures in the prediction of group membership, and whether combining them with cortical thickness and white matter fractional anisotropy further improved accuracy.

RESULTS: The GM-NDI was significantly lower in temporal pole, anterior parahippocampal gyrus, and hippocampus of the schizophrenia patients than the healthy controls. The GM-NDI of patients with bipolar I disorder did not differ significantly from either schizophrenia patients or healthy controls, and it was intermediate between the two groups in the post hoc analysis. Regardless of diagnosis, higher performance in spatial working memory was significantly associated with higher GM-NDI mainly in the frontotemporal areas. The addition of GM-NDI to cortical thickness resulted in higher accuracy to predict group membership.

CONCLUSIONS: GM-NDI captures brain differences in the major psychoses that are not accessible with other structural magnetic resonance imaging methods. Given the strong association of GM-NDI with disease state and neurocognitive performance, its potential utility for biological subtyping should be further explored.

Keywords: Bipolar disorder, GBSS, Gray matter microstructure, Neuritic density, NODDI, Schizophrenia

http://dx.doi.org/10.1016/j.biopsych.2016.12.005

Excessive synaptic pruning during adolescence and associated dendritic abnormalities have been implicated as a key pathophysiological process involved in major psychoses (1–4). Consistent with this hypothesis, postmortem studies of gray matter (GM) neuritic microstructure have shown lower dendritic marker (microtubule-associated protein 2 [MAP2]) density (5,6), dendritic tree arborization (7,8), and spine density (7,9,10) in individuals with schizophrenia. Although it has not been investigated as thoroughly, similar deficits in MAP2, dendritic spine density, and dendritic length have been reported in bipolar disorder (11,12). However, conflicting observations, limited number of brain regions examined, small sample sizes, and potential alterations during the postmortem interval before tissue fixation can limit interpretation of postmortem studies (2,13). In vivo neuroimaging of these neural substrates could provide opportunity for new knowledge of the neurobiological underpinnings of severe mental illnesses.

Previous studies of psychiatric disorders have typically focused on analysis of white matter (WM) microstructure using diffusion tensor imaging (14). However, recent advances in diffusion-weighted magnetic resonance imaging (MRI) acquisition and modeling have made it possible to examine GM microstructure in vivo (15–17). Neurite orientation dispersion and density imaging (NODDI) is a recently introduced biophysical diffusion modeling approach that approximates neurites (axons and dendrites) as a set of sticks with zero radii to capture the extremely restricted diffusion perpendicular to the neurites and unhindered diffusion along them (15). Thus, NODDI is well suited for microstructural modeling of GM tissue, which is primarily composed of dendritic trees and crossing axons, because it permits high dispersion of the neuritic orientations (15,18). This technique characterizes 1) the spatial configuration of the neurites with the orientation dispersion index (ODI) and 2) tissue microstructural composition with

SEE COMMENTARY ON PAGE e71

 ISSN: 0006-3223

the neuritic density index (NDI), the volume fraction of neurites in brain tissue (15). We have recently shown in healthy individuals that these measures are sensitive to GM changes caused by aging, associated with cognitive performance, and are a better predictor of chronological age than cortical thickness or WM microstructure (19).

Robust differences in GM structural MRI and WM diffusion tensor imaging indices have been documented between individuals with schizophrenia or bipolar disorder and healthy individuals (20,21). However, these methods alone have been unable to fully discriminate between the diagnostic groups (22). Moreover, structural MRI studies have not consistently shown a strong association between GM macrostructure and cognitive deficits in schizophrenia or bipolar I disorder (BDI) (23). Although unique pathophysiological factors are likely involved in schizophrenia and BDI, these two disorders share some genetic risks, underlying pathology, and clinical symptoms (24,25). Using NODDI to characterize GM microstructure, our primary objective was to assess potential differences among individuals with schizophrenia, those with BDI, or those who are healthy (19,26). The majority of the neuropathological findings described in people with schizophrenia and BDI are located in the frontal and temporal lobes (27), and we therefore hypothesized that we would find neuritic abnormalities in the same areas among individuals with schizophrenia and BDI, but with smaller effects in those with BDI. Second, given that these regions are known to be involved in higher cognition, we also assessed the association between GM microstructure and cognitive performance. Finally, we conducted exploratory classification analysis to assess the diagnostic accuracy of NODDI-derived GM microstructural measures in isolation and in combination with other imaging metrics.

METHODS AND MATERIALS

Participants

Individuals with schizophrenia (n = 36) or BDI (n = 29) and healthy individuals of comparable age and sex (n = 35) were recruited at the Centre for Addiction and Mental Health in Toronto, Ontario, Canada (Table 1). All participants were administered the Structured Clinical Interview for DSM-IV-TR for Axis-I disorders and interviewed by a psychiatrist. The schizophrenia group comprised participants with a diagnosis of either schizophrenia or schizoaffective disorder who were assessed using the Positive and Negative Syndrome Scale. Participants with BDI were euthymic based on their scores on the Young Mania Rating Scale (<10) and Hamilton Depression Rating Scale (<10). The BDI group was enriched with patients with a positive history for psychosis (Table 1). To verify absence of a substance use disorder, a urine toxicology screen was obtained. Individuals with a positive urine toxicology screen, current substance abuse, a history of substance dependence within the past 6 months, and a history of severe head trauma (with loss of consciousness or

Table 1. Demographic, Cognitive, and Clinical Characteristics of the Participants[a]

	HC (n = 35)	SZ (n = 36)	BDI (n = 29)
Age, Years, Mean (SD) [Range]	33.6 (12.4) [20–56]	35.5 (8.4) [20–55]	31.5 (11.0) [20–56]
Sex, Female/Male	16/19	17/19	15/14
Education, Years, Mean (SD)	15.3 (2.2)	13.6 (2.1)	14.6 (1.7)
Ethnicity	23 white, 1 AC, 2 H, 7 Asian, 2 other	23 white, 9 AC, 2 H, 2 other	27 white, 2 Asian
HVLT-R, Mean (SD)	26.7 (4.7)	22.5 (5.8)	25.7 (2.6)
LNS, Mean (SD)	16.5 (2.5)	13.3 (2.8)	16.0 (2.0)
SSP, Mean (SD)	18.1 (3.7)	15.4 (3.4)	16.0 (2.7)
CPT-IP, Mean (SD)	3.1 (0.6)	2.3 (0.7)	2.5 (0.6)
BACS-SDC, Mean (SD)	65.1 (15.7)	52.1 (14.2)	53.7 (12.1)
DWI Motion, RMS, Mean (SD)	1.30 (0.27)	1.29 (0.26)	1.25 (0.30)
Age of Onset, Years, Mean (SD)	—	22.2 (5.5)	20.7 (6.1)
Disease Duration, Years, Mean (SD)	—	13.8 (9.3)	11.4 (9.3)
Disease Subtypes	—	27 SZ, 9 SZaff (5 BD type, 2 depressive type, 2 unknown)	23 psychotic, 5 nonpsychotic, 1 unknown
Chlorpromazine Equivalent, mg/day, Mean (SD)	—	314 (341)	212 (312)
Lithium Carbonate, mg/day, Mean (SD)	—	—	705 (618)
PANSS Positive, Mean (SD)	—	12.1 (4.7)	—
PANSS Negative, Mean (SD)	—	11.6 (3.2)	—
PANSS General, Mean (SD)	—	23.8 (6.0)	—
HDRS, Mean (SD)	—	—	4.6 (2.6)
YMRS, Mean (SD)	—	—	2.0 (2.0)

AC, African Canadian; BACS-SDC, Brief Assessment of Cognition in Schizophrenia, symbol-coding subtest; BDI, bipolar I disorder; CPT-IP, Continuous Performance Test, Identical Pairs; DWI, diffusion-weighted imaging; H, Hispanic; HC, healthy controls; HDRS, Hamilton Depression Rating Scale; HVLT-R, Hopkins Verbal Learning Test-Revised; LNS, Letter-Number Sequence; PANSS, Positive and Negative Syndrome Scale; RMS, root mean square deviation (in mm); SSP, spatial span; SZ, schizophrenia; SZaff, schizoaffective disorder; YMRS, Young Mania Rating Scale.

[a]Between-group comparisons for demographic and cognitive characteristics are presented in Supplemental Table S7.

trauma-induced seizure) or neurological disorders (including dementia) were excluded. For healthy participants, a history of a schizophrenia spectrum disorder in a first-degree family member was also an exclusion criterion. The study was approved by the Centre for Addiction and Mental Health Ethics Review Board, and all participants provided written informed consent after receiving a full explanation of the study.

Cognitive Testing

Cognitive performance was assessed using the MATRICS Consensus Cognitive Battery (28). In this study, we focused on five cognitive domains in which people with schizophrenia and BDI have shown impairment in meta-analyses of neurocognitive data (29–32): 1) attention (Continuous Performance Test-Identical Pairs); 2) verbal learning (Hopkins Verbal Learning Test-Revised); 3) verbal working memory (Letter-Number Sequence); 4) spatial working memory (spatial span); and 5) processing speed (Brief Assessment of Cognition in Schizophrenia, symbol coding subtest).

Magnetic Resonance Image Acquisition

All MR images were collected on a 3T GE Discovery MR750 system (General Electric, Milwaukee, WI) using an eight-channel head coil. Diffusion-weighted data were acquired using a single shot dual-spin echo planar imaging sequence with three different b values (i.e., 3 shells; 30 directions each): 1000 s/mm^2, 3000 s/mm^2, and 4500 s/mm^2 with two excitations to increase the signal-to-noise ratio; along with five interspersed b_0 images for each diffusion-weighted shell. The acquisition parameters were echo time 108 ms, repetition time 12,000 ms, resolution 2 × 2 × 2 mm^3, 82 slices, and acquisition matrix 128 × 128. Sixty-direction single-shell (b value = 1000 s/mm^2 with 5 b_0 images) diffusion-weighted dual-spin echo planar images were also acquired with the following parameters: echo time 85 ms, repetition time 8800 ms, resolution of 2 × 2 × 2 mm^3, 73 slices, and acquisition matrix 128 × 128. T1-weighted structural images were acquired using a three-dimensional inversion-prepared fast spoiled gradient-recalled echo acquisition protocol with an echo time of 3 ms, repetition time of 6.7 ms, inversion time of 650 ms, flip angle 8°, and resolution of 0.9 × 0.9 × 0.9 mm^3.

Diffusion-Weighted MRI Processing

Four-dimensional multishell diffusion-weighted images were corrected for motion-related misalignments and eddy current distortions using the *eddy_correct* function in FSL (version 5.0.6; available at http://www.fmrib.ox.ac.uk/fsl) (33). A brain mask was generated from the b_0 images using the Brain Extraction Tool (34). Next, the diffusion tensor model was fitted voxel by voxel within the brain mask using the *dtifit* function (part of FSL) to calculate fractional anisotropy (FA) maps (only performed in b = 1000 images).

NODDI is a recently introduced biophysical diffusion modeling approach that uses diffusion-weighted MR images acquired at multiple degrees of diffusion-weighting (multiple b values) to distinguish three microstructural subcomponents: intracellular (neuritic), extracellular, and cerebrospinal fluid (CSF) compartments (15). The NODDI-MATLAB toolbox (available at https://www.nitrc.org/projects/noddi_toolbox/) was used to generate the following parameter maps: 1) fraction of CSF (f_{CSF}), which indexes the volume fraction of Gaussian isotropic diffusion (free fluid) within each voxel; 2) NDI, which indicates the fraction of tissue water restricted within neuritis (axons and dendrites) in the non-CSF compartment; and 3) ODI, which characterizes spatial configuration of neurites and ranges from 0 (no neuritic dispersion) to 1 (full dispersion) (15). The *Rmsdiff* function (implemented in FSL) was used to estimate the average relative root mean square distance as a measure of motion between the consecutive diffusion-weighted volumes.

GM-Based Spatial Statistics

NODDI GM-based spatial statistics (NODDI-GBSS) to perform voxelwise statistical analysis on GM microstructure has been described elsewhere in more detail (19,26). Briefly, GM fraction maps were estimated in the native diffusion space by subtracting CSF fraction (f_{CSF} maps from NODDI) and WM fraction [estimated by two-tissue class segmentation of FA images using *Atropos* (35)] from 1 in each voxel (19). To increase tissue contrasts and enhance between-subject registration steps, partial volume estimation maps for each tissue class were multiplied by their corresponding contrast (0 for CSF, 1 for GM, and 2 for WM) and summed together to generate images with similar contrast to T1-weighted images (19). The resulting images were then used to build a study-specific template using the *buildtemplateparallel.sh* script in Advanced Normalization Tools (36,37). GM fraction, ODI, and NDI images were warped to the template space using the warp fields estimated during the previous step (*gbss_1_reg.sh* script; Figure 1). To enhance between-subject alignment of GM voxels, GBSS adopts the tract-based spatial statistics algorithm (38). The average GM fraction map was skeletonized, and for each subject, diffusion metrics (i.e., ODI and NDI) and GM fraction were projected from local voxels with greatest GM fraction in the template space onto the skeleton. The final skeleton was generated by keeping only voxels with a GM fraction > 0.65 in > 75% of the subjects (*gbss_2_skell.sh* script; Figure 1). The remaining voxels on the subjects' skeletons with nonsatisfactory GM fraction (<0.65) were filled with the average of the surrounding satisfactory voxels on the skeleton (GM fraction >0.65) weighted by their closeness with a Gaussian kernel (σ = 2 mm; *gbss_3_fill.sh* script). The GBSS pipeline scripts are free online (available at https://github.com/arash-n/GBSS).

Voxelwise permutation analysis was carried out on GBSS-derived skeletonized NODDI parameter maps (ODI and NDI) across participants using Randomise (39). Threshold-free cluster enhancement was used for each permutation analysis (n = 10,000) to determine brainwide statistical significance fully corrected for multiple comparisons (familywise error [FWE]–corrected p) without defining an arbitrary cluster threshold (40).

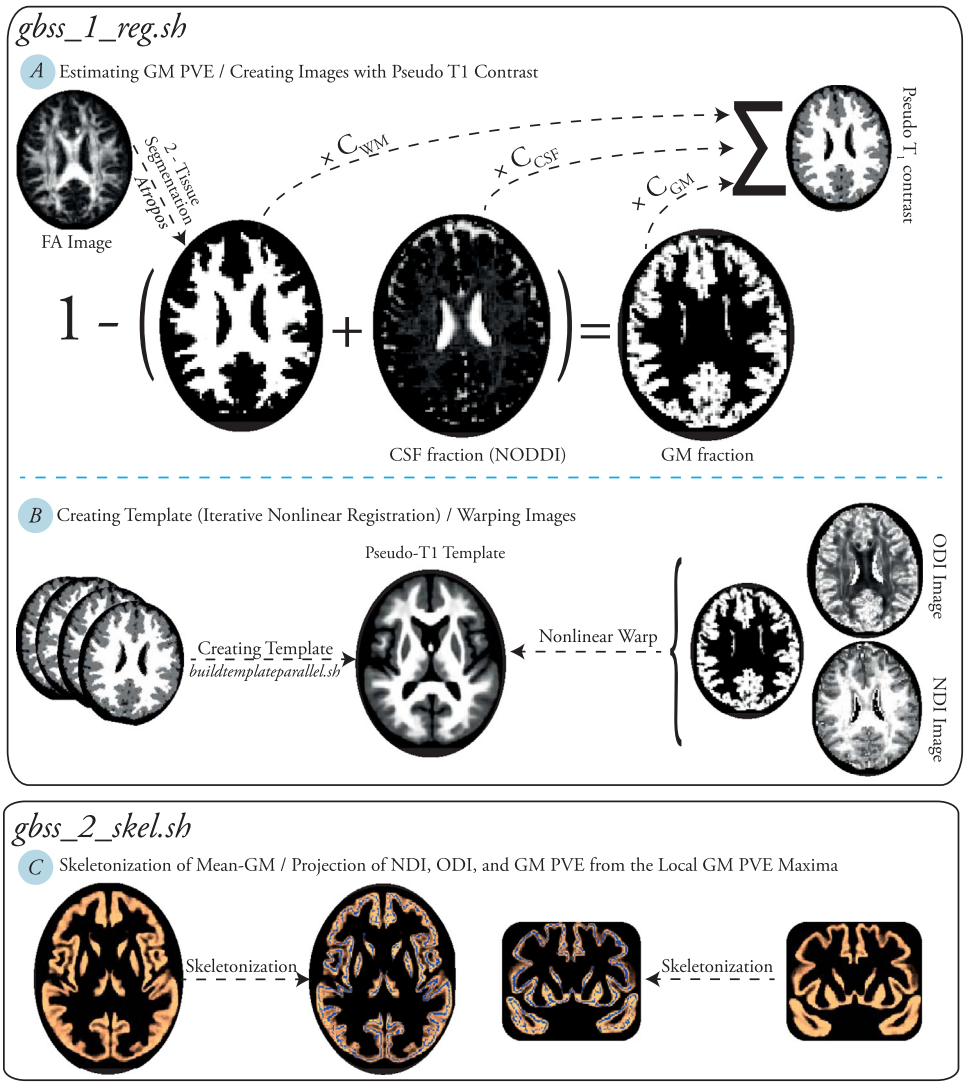

Figure 1. Overview of neurite orientation dispersion and density imaging (NODDI) gray matter (GM)–based spatial statistics pipeline (*gbss_1_reg.sh* and *gbss_2_skel.sh* scripts). **(A)** White matter (WM) fraction was estimated by applying two-tissue segmentation on fractional anisotropy (FA) maps (*Atropos* function in Advanced Normalization Tools), whereas GM fraction was estimated by subtracting white matter and cerebrospinal fluid (CSF) fractions from one. Finally, images with a pseudo-T1 contrast were generated for registration steps. **(B)** A norm template was generated by iterative nonlinear registration of pseudo-T1 images (*buildtemplateparallel.sh* script in Advanced Normalization Tools). Maps generated using NODDI (neurite density index [NDI] and orientation dispersion index [ODI] images) and GM fraction maps were warped to the template space. **(C)** GM fraction maps were averaged across subjects. In the template space, mean GM image was skeletonized and NDI, ODI, and GM fraction were projected onto the skeleton from the local GM fraction maxima. PVE, partial volume estimation.

Tract-Based Spatial Statistics for White Matter FA

The tract-based spatial statistics algorithm was used to conduct whole-brain voxelwise analysis for the WM-FA (38). As described above for the GBSS analysis, permutation-based voxelwise statistics were carried out using Randomise.

Cortical Thickness and Surface Area Analysis

Structural T1-weighted images for all participants were submitted to the CIVET-pipeline (v 1.1.10; available at http://www.bic.mni.mcgill.ca/ServicesSoftware/CIVET) for preprocessing (registration, bias-field correction, and tissue classification), generating cortical models, and vertexwise cortical thickness and surface area estimation as previously described (41). Vertexwise analyses were conducted using the RMINC package (https://github.com/Mouse-Imaging-Centre/RMINC). Results were corrected for multiple comparisons using false discovery rate (FDR) correction.

Statistical Analyses

For both voxelwise (GBSS and TBSS) and vertexwise (cortical morphology from CIVET) analyses, the following effects were tested on GM and WM microstructure along with cortical thickness/surface area: 1) effects of diagnoses independent of age and sex (FWE-corrected [GM-NODDI parameters and WM-FA] and FDR-corrected p [cortical thickness] $< .017$ [0.05/3] were considered significant after Bonferroni correction for 3 between-diagnosis contrasts) and 2) effects of cognitive tasks with adjustment for age, sex, and diagnosis (FWE-corrected and FDR-corrected $p < .01$ [0.05/5] were deemed significant after Bonferroni correction for five cognitive tasks).

For post hoc analyses and to compare diagnostic accuracy of GM microstructural and macrostructural measures, all voxels/vertices from voxelwise/vertexwise analyses that showed a significant effect of diagnosis were selected (corrected $p < .05$). For each participant, for each modality a single parameter was extracted from those voxels/vertices by

averaging values in GM skeleton (NODDI parameters), WM skeleton (FA), and cortical vertices (cortical morphology measures). The resulting average values were used to predict diagnosis using logistic regression models while controlling for the effects of age and sex. Improvement of area under the curve (AUC) for the receiver operating characteristic curves for multimodal models relative to unimodal models, as well as NODDI measures versus other modalities were assessed using bootstrapping (n = 10,000; one-sided $p < .05$ was considered significant improvement; pROC package in R software [version 3.0.2]) (42). AUCs > 0.90 were considered excellent, > 0.80 good, > 0.70 satisfactory, and < 0.70 poor. All post hoc region of interest analyses were conducted using R software.

Exploratory between-modality correlation analyses were performed for the modalities that showed a significant effect of diagnosis using the results of cortical regional parcellations and deterministic tractography (Supplemental Methods).

RESULTS

Effect of Diagnosis on GM Microstructure

Compared to healthy participants, individuals with schizophrenia demonstrated significantly lower GM-NDI in left (peak FWE $p = .004$) and right (peak FWE $p = .003$) rostromedial temporal lobe structures (i.e., the temporal pole, anterior parahippocampal gyrus, and hippocampus; Figure 2A; Supplemental Table S1). A trend toward higher ODI in patients with schizophrenia relative to healthy individuals was observed in the bilateral precuneus, left posterior cingulate cortex, supplementary motor area, and lateral occipital cortex (FWE $p < .05$; Supplemental Figure S1). No significant differences in GM-NDI and GM-ODI were observed between persons with BDI and persons with schizophrenia or healthy participants.

Exploratory analysis showed a trend for sex by diagnosis (schizophrenia vs. BDI) interaction effect (FWE $p < .05$) on dorsolateral prefrontal cortical (DLPFC) NDI (peak FWE $p = .02$ in the left frontal pole; Supplemental Figure S2). Further details can be found in Supplemental Results.

Post Hoc Analyses

After conducting GBSS across the brain, we used the voxels showing significantly lower NDI in patients with schizophrenia relative to healthy controls (FWE $p < .05$) as the region of interest for the following post hoc analyses.

Average GM-NDI extracted from the region of interest was significantly different between all groups (schizophrenia < BDI < healthy; schizophrenia < healthy: $p = 1.3 \times 10^{-10}$, BDI < healthy: $p = .005$, schizophrenia < BDI: $p = 2.8 \times 10^{-5}$; Figure 2B). Effects of diagnoses on average NDI did not show substantial change after adjusting for head motion during diffusion-weighted imaging (schizophrenia < healthy: $p = 6.9 \times 10^{-11}$; BDI < healthy: $p = .0037$; schizophrenia < BDI: $p = 2.1 \times 10^{-5}$). A subanalysis among white participants also demonstrated similar group differences (schizophrenia < healthy: $p = 1.9 \times 10^{-7}$; BDI < healthy: $p = .021$; schizophrenia < BDI: $p = 2.8 \times 10^{-5}$). To mitigate potential concerns regarding the long-term effects of medication or duration of illness, we further performed the same analysis in individuals ≤35 years of age. Similar results were found among this subset of individuals (schizophrenia < healthy: $p = 2.8 \times 10^{-6}$; BDI < healthy: $p = .012$; schizophrenia < BDI: $p = .002$).

Further analysis revealed that average GM-NDI was not associated with chlorpromazine-equivalent antipsychotic dosage among participants with either schizophrenia ($\beta = -0.08$, $p = .67$) or BDI ($\beta = 0.09$, $p = .64$). Furthermore, no difference was detected between patients who were not receiving antipsychotic treatment (BDI: $n = 7$; schizophrenia: $n = 7$) and patients taking antipsychotic medications ($p = .43$, Supplemental Figure S3). Among patients with BDI, lithium therapy (binary variable, $p = .12$) and lithium carbonate dosage ($p = .7$) were not associated with average NDI (nine BDI patients were not taking lithium at the time of the study).

When we separated patients with schizoaffective diagnoses from the schizophrenia group, both groups of patients showed significantly lower GM-NDI than healthy controls (schizoaffective: $p = 1.4 \times 10^{-5}$; schizophrenia: $p = 5.3 \times 10^{-9}$) and BDI patients (schizoaffective: $p = 6.2 \times 10^{-4}$; schizophrenia: $p = 9.0 \times 10^{-5}$). No significant difference was observed between schizoaffective and schizophrenia patients in GM-NDI ($p = .28$; Supplemental Figure S3). Furthermore, we did not observe a significant difference in GM-NDI between BDI patients with and without a history of psychosis (mean $NDI_{psychotic}$ [SD] = 0.351 [0.015]; mean $NDI_{nonpsychotic}$ [SD] = 0.357 [0.021]; $p = .75$).

Associations With Cortical Macrostructure and WM-FA

Schizophrenia participants demonstrated significantly lower cortical thickness than healthy participants in bilateral DLPFC, medial frontal, orbitofrontal and fusiform cortices, left angular gyrus, posterior cingulate cortex and frontal pole, and right middle temporal gyrus, occipital pole, and temporal pole (FDR $p < .017$; Figure 2C). No significant differences were observed in comparisons between other diagnostic groups. Regional cortical surface area did not differ significantly among the diagnostic groups.

Compared to healthy controls, participants with schizophrenia showed significantly lower FA throughout the WM (FWE $p < .017$; Figure 2D), with the greatest deficit observed in the body and genu of corpus callosum (peak FWE $p = .002$; Supplemental Table S2). There were no significant differences in FA values between participants with BDI and either those with schizophrenia or those who were healthy.

Results for exploratory analyses assessing correlations between each cortical area's NDI with the same area's cortical thickness and the FA from corpus callosum projecting to the corresponding lobe can be found in Supplemental Results.

Associations With Cognitive Performance

While adjusting for the effects of diagnosis, age, and sex, better performance in spatial span was significantly associated with higher GM-NDI in several GM areas, such as the DLPFC; orbitofrontal, medial prefrontal, superior temporal, and cingulate cortices; and temporal pole, insula, hippocampus, and striatum (FWE $p < .01$; peak FWE $p = .002$; Figure 3A; Supplemental Table S3). Post hoc analysis showed that

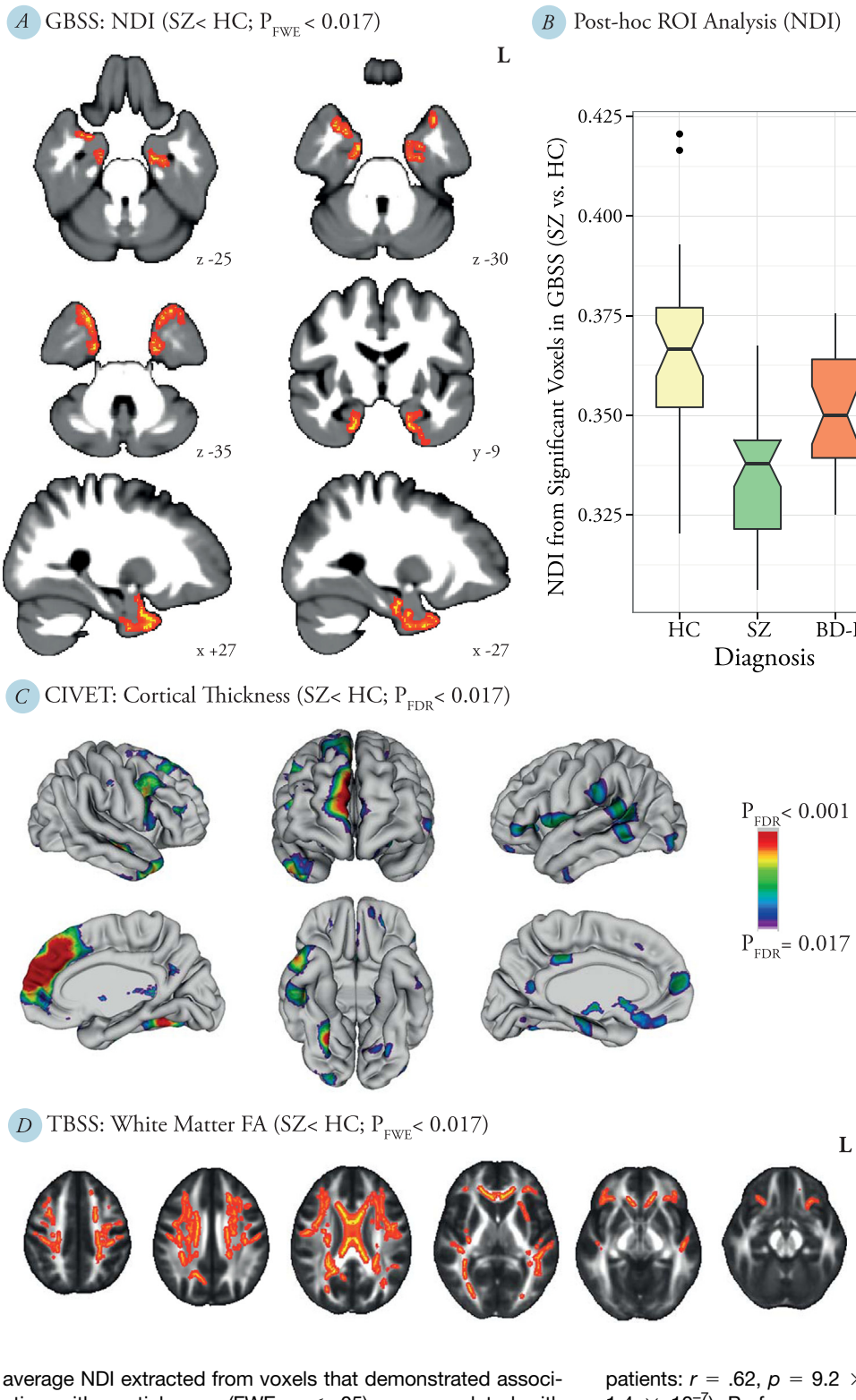

Figure 2. **(A)** Gray matter regions showing lower neuritic density index (NDI) among schizophrenia patients (SZ) relative to healthy participants (HC) (familywise error [FWE] $p < .017$) in gray matter–based spatial statistics (GBSS). **(B)** Post hoc analysis showing group differences in NDI extracted from voxels showing lower NDI in GBSS (SZ vs. HC); FWE $p < .05$). **(C)** Regions showing lower cortical thickness in SZ patients in comparison to HCs (false discovery rate [FDR] $p < .017$). **(D)** Tract-based spatial statistics (TBSS) results showing white matter regions with lower fractional anisotropy (FA) among SZ patients vs. HCs (FWE $p < .017$). BDI, bipolar I disorder; L, left; ROI, region of interest.

average NDI extracted from voxels that demonstrated association with spatial span (FWE $p < .05$) was correlated with performance in this cognitive domain in all three diagnostic groups (partial correlation coefficients, controlled for age, healthy participants: $r = .73$, $p = 2.0 \times 10^{-6}$; schizophrenia patients: $r = .62$, $p = 9.2 \times 10^{-5}$; BDI patients: $r = .84$, $p = 1.4 \times 10^{-7}$). Performances in the other cognitive tasks were not associated with GM-NDI.

We did not observe any association between cortical thickness and any of the cognitive tests in our sample.

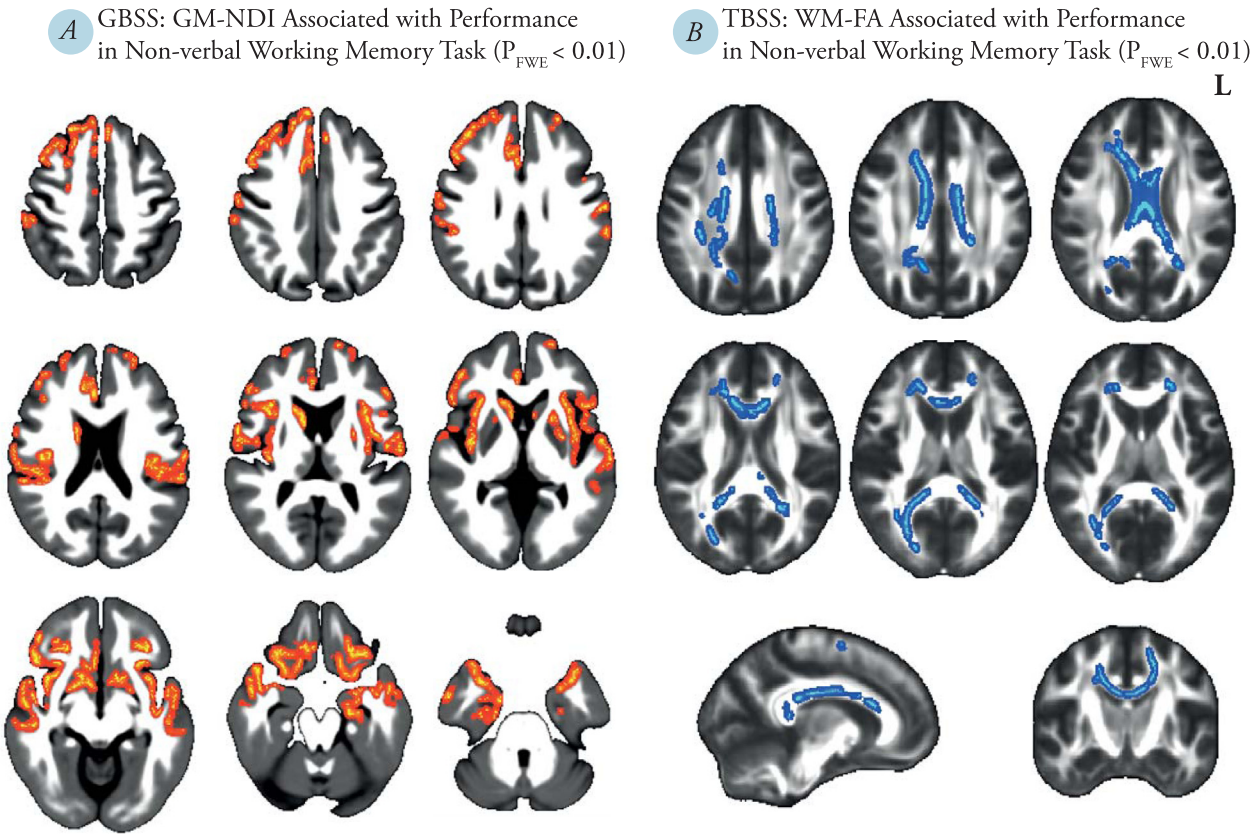

Figure 3. **(A)** Gray matter (GM) regions demonstrating significantly higher (familywise error [FWE] $p < .01$) neuritic density index (NDI) with better performance in spatial span (a spatial working memory task) across all participants in gray matter–based spatial statistics (GBSS). **(B)** White matter (WM) regions demonstrating significantly higher (FWE $p < .01$) fractional anisotropy (FA) with better performance in spatial span across all participants in tract-based spatial statistics (TBSS).

However, better performance in spatial span was associated with higher WM-FA (peak FWE $p = .005$ at corpus callosum; Figure 3B; Supplemental Table S4). Similar to GM-NDI, WM-FA was not significantly associated with performance in other cognitive tasks.

Exploratory Classification Analyses Using Logistic Regression Models

For each modality, a single parameter (average GM-NDI, WM-FA, and cortical thickness from voxels/vertices that differed significantly between participants with schizophrenia and healthy controls) was used to predict diagnosis using logistic regression analysis and receiver operating characteristic curves, while adjusting for age and sex (Figure 4).

Schizophrenia vs. Healthy Participants. As expected, all three modalities individually showed good to excellent diagnostic accuracy (NDI: AUC = 0.93, $p = 8.6 \times 10^{-5}$; cortical thickness: AUC = 0.85, $p = 3.0 \times 10^{-5}$; FA: AUC = 0.87, $p = 3.0 \times 10^{-5}$). Combining all three measures significantly improved accuracy only relative to the cortical thickness and FA unimodal models (AUC = 0.95; Supplemental Table S5). Moreover, FA no longer significantly contributed to the multimodal model (NDI: $p = .01$; cortical thickness: $p = .013$; FA: $p = .4$).

Schizophrenia vs. BDI. All three measures demonstrated good accuracy between the diagnostic groups in the unimodal models (NDI: AUC = 0.82, $p = 6.3 \times 10^{-4}$; cortical thickness: AUC = 0.82, $p = .0013$; FA: AUC = 0.80, $p = .0023$). Combining the three measures significantly improved accuracy relative to all unimodal models (AUC = 0.90; Supplemental Table S5). In the multimodal model, NDI and cortical thickness significantly contributed to the differentiation between schizophrenia and BDI participants (NDI: $p = .03$; cortical thickness: $p = .012$; FA: $p = .36$).

BDI vs. Healthy Participants. NDI and FA showed satisfactory accuracy, whereas cortical thickness demonstrated a poor accuracy in the unimodal classification models (NDI: AUC = 0.72, $p = .0086$; cortical thickness: AUC = 0.59, $p = .4$; FA: AUC = 0.70, $p = .03$). Improvement was observed with the multimodal model only relative to the cortical thickness unimodal model (AUC = 0.73; Supplemental Table S5).

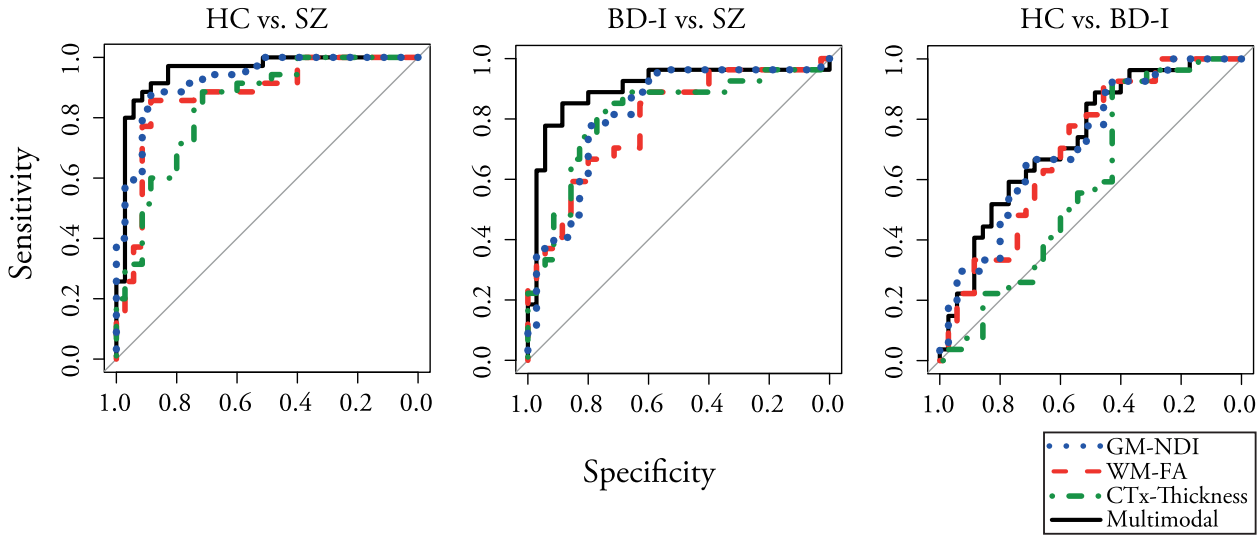

Figure 4. Receiver operating characteristic curves predicting diagnosis (left: schizophrenia [SZ] vs. healthy controls [HC]; middle: SZ vs. bipolar I disorder [BDI]; right: BDI vs. HC; dashed red line: white matter fractional anisotropy (WM-FA); dotted line dark blue: gray matter neuritic density index (GM-NDI); dashed-dotted green line: cortical thickness (CTx); solid black line: combined [GM-NDI + cortical thickness + WM-FA]).

Finally, GM-NDI tended to be a stronger separator than cortical thickness in distinguishing between schizophrenia and healthy individuals ($p = .043$), as well as between BDI and healthy individuals ($p = .044$; Supplemental Table S6).

DISCUSSION

We used NODDI to characterize and compare GM microstructure in participants with schizophrenia, BDI, and healthy controls. We found a significant reduction in NDI in the temporal pole and hippocampus in participants with schizophrenia compared to healthy controls. The neuritic density of participants with BDI was intermediate (i.e., lower than in healthy participants and higher than in participants with schizophrenia); however, these differences were not significant in our brain-wide analysis. Regardless of diagnosis, NDI was related to neurocognitive performance. Finally, when three neuroimaging measures were considered—GM-NDI, cortical thickness, and WM-FA—NDI provided superior accuracy in discriminating between schizophrenia and healthy participants. The combination of the three measures improved the discrimination between schizophrenia and BDI participants. These results suggest that NDI is a potentially useful new biological marker of schizophrenia that can be used alone or combined with other neuroimaging biomarkers to differentiate diagnostic groups.

NDI in the temporal pole, hippocampus, and parahippocampus was lower in participants with schizophrenia than in healthy controls. Voxelwise analysis did not detect any significant difference between individuals with BDI and schizophrenia or healthy individuals. However, NDI extracted from voxels demonstrating lower NDI in schizophrenia significantly contributed to discrimination between BDI versus schizophrenia as well as BDI versus healthy participants. In addition, exploratory analysis showed that GM-NDI deficits in BDI patients might be sex specific. Our findings suggest that neuritic density deficits may serve as a common biomarker for these major psychotic illnesses while at the same time suggesting that schizophrenia patients show more severe deficits relative to BDI patients. To date, few postmortem studies have investigated microstructural abnormalities in BDI (11). Additional postmortem studies on BDI are required to unravel the pattern of neuritic deficits in patients with BDI and the role of sex in this disorder.

We found that abnormalities in GM macrostructure (cortical thickness) and microstructure (neuritic density) were nonoverlapping. In addition, we found that cortical GM neuritic density is largely independent of cortical thickness in the same area and WM microstructure projecting to that area (as indexed by corpus callosum FA). The four significant associations found between cortical thickness and NDI were inverse relationships, yet both NDI and cortical thickness were lower in patients with schizophrenia, supporting the likelihood of independence of these variables. These results suggest that GM microstructure (NDI) may capture unique histopathological features of schizophrenia.

Although GM-NDI tended to be a stronger separator than cortical thickness in distinguishing between schizophrenia and BDI versus healthy controls, these results should be regarded as preliminary findings and need to be further verified in future studies. When combined, GM-NDI and cortical thickness independently contributed to the models differentiating schizophrenia participants from healthy controls or from BD-I participants. Multimodal models could therefore enhance the differentiation of these diagnostic groups. Multivariate pattern recognition methods using cortical macrostructural and WM microstructural biomarkers of schizophrenia have been used to predict diagnosis (43) and sources of heterogeneity within the disease (44). The addition of GM microstructural measures in these multimodal approaches may further enhance their diagnostic accuracy and reveal neural correlates of heterogeneity within each diagnostic group.

Axons and dendrites occupy a similar fraction of the GM neuropil volume (45). Therefore, deficits in dendritic density, axonal density, or both may explain the NDI deficit we observed in the hippocampus, temporal pole, and parahippocampal cortices in schizophrenia. Although conflicting findings have been reported (13), our findings of decreased hippocampal and parahippocampal neuritic density are congruent with the results of neuropathological studies of schizophrenia indicating lower MAP2 (a cytoskeletal protein primarily located in dendrites and cell bodies) immunoreactivity mainly in the hippocampus and associated areas (5,13,46). Other postmortem studies have suggested lower prefrontal (11) and temporal (10) dendritic spine density in schizophrenia. We observed cortical thickness reductions but not NDI reductions in prefrontal cortex in schizophrenia participants in our study. Thus, the relevance of primary dendritic abnormalities (indexed by MAP2 immunoreactivity, dendritic length, etc.) versus dendritic spine density may require direct correlation of NDI with histological findings in postmortem studies.

Throughout the frontotemporal cortical areas, higher NDI was associated with better performance in spatial working memory. Functional MRI studies in healthy individuals have shown that some of these regions become consistently activated during working memory tasks (e.g., insula and DLPFC) or are responsive to working memory load (e.g., cingulate gyrus and temporal areas) (47). Numerous functional MRI studies of working memory have also implicated dysfunction in DLPFC and anterior cingulate cortices in schizophrenia (48). Like WM-FA, GM-NDI was significantly associated only with spatial working memory among the cognitive domains included in this study. This may be partly explained by other confounders, such as medication effects that may obscure the relationship between those cognitive tests and brain microstructure (31). In addition, greater genetic influence and weaker diagnosis-related moderator effects on spatial working memory relative to verbal learning and verbal working memory may result in stronger association between these neuroimaging markers and spatial working memory (49). Spatial working memory impairment is present in relatives and twins discordant for schizophrenia (50), and it has been proposed as a cognitive endophenotype for schizophrenia (51,52). Considering the recent evidence suggesting that schizophrenia risk variants may influence dendritic microstructure (4), future studies should explore the usefulness of NDI as an intermediate phenotype for genetic risk factors of schizophrenia (53).

Several limitations of this study deserve discussion. First, most participants with schizophrenia and BDI had previous or current exposure to antipsychotic medications. It has been shown that antipsychotic medications do not affect dendritic structures in rats (11). Moreover, similar group differences were observed in younger patients with less disease chronicity (i.e., less cumulative drug exposure), and there was no association between NDI and current antipsychotic medication dosage in either participants with schizophrenia or BDI. However, future studies on drug-naïve patients would be useful. Second, a larger sample size might have allowed for detection of effect in other brain regions, or of possible smaller effects in BDI participants. Third, although the male-female ratio among patients with schizophrenia was consistent with epidemiological findings, our inclusion of schizoaffective patients created an approximate 1:1 male-female ratio (54). Although we did not observe significant differences between clinical subtypes of schizophrenia spectrum disorders (i.e., schizophrenia and schizoaffective disorder) in our post hoc analysis, future studies with large sample sizes for both subtypes are necessary to elucidate potential differences between these diagnostic groups across the brain. Finally, the prediction models comparing accuracy of GM-NDI and other modalities should be viewed as a proof of concept analysis. More rigorous studies using machine-learning techniques with separate test-sets could elucidate the true utility of NDI as a diagnostic biomarker for schizophrenia and BDI.

In summary, our study suggests that novel diffusion-weighted MRI acquisition and modeling techniques such as multishell diffusion imaging and NODDI may be useful in vivo neuroimaging approaches to study the histopathology underlying central nervous system disorders. NODDI-driven microstructural indices may be more robust biomarkers than established neuroimaging biomarkers for psychiatric illnesses and cognitive performance.

ACKNOWLEDGMENTS AND DISCLOSURES

This work was supported by a Canadian Institutes of Health Research fellowship award (to AN). TKR has received research support from Brain Canada, Brain and Behavior Research Foundation, Canada Foundation for Innovation, Canada Research Chair, Canadian Institutes of Health Research, Ontario Ministry of Health and Long-Term Care, Ontario Ministry of Research and Innovation, the US National Institutes of Health, and the W. Garfield Weston Foundation. LS is funded by the Ontario Graduate Scholarship Program (Faculty of Medicine, University of Toronto). TR is funded by the Isabel Johnson Biomedical Postdoctoral Award, Alzheimer Society of Canada Research Program. ANV is funded by the Canadian Institutes of Health Research, Ontario Mental Health Foundation, Brain and Behavior Research Foundation, and the National Institute of Mental Health (Grant Nos. R01MH099167 and R01MH102324).

BHM directly owns General Electric stock (<$5000). All other authors report no biomedical financial interests or potential conflicts of interest.

ARTICLE INFORMATION

From the Kimel Family Translational Imaging-Genetics Laboratory (AN, MLL, JP, LS, SS, TR, ANV), Research Imaging Centre (AN, MLL, JP, LS, SS, TR, SC, ANV), Campbell Family Mental Health Research Institute, Centre for Addiction and Mental Health; Department of Psychiatry (AN, BHM, TKR, MLL, TR, ANV) and Institute of Medical Science (TKR, LS, SS, ANV), University of Toronto; and Neurosciences and Mental Health (ALW), The Hospital for Sick Children, Toronto, Ontario, Canada.

Address correspondence to Aristotle N. Voineskos, M.D., Ph.D., Kimel Family Translational Imaging-Genetics Laboratory, Research Imaging Centre, Campbell Family Mental Health Research Institute, Centre for Addiction and Mental Health, 250 College Street, Toronto, ON, Canada M5T1R8; E-mail: Aristotle.Voineskos@camh.ca.

Received Jun 14, 2016; revised Oct 26, 2016; accepted Dec 1, 2016.

Supplementary material cited in this article is available online at http://dx.doi.org/10.1016/j.biopsych.2016.12.005.

REFERENCES

1. Keshavan MS, Anderson S, Pettergrew JW (1994): Is schizophrenia due to excessive synaptic pruning in the prefrontal cortex? The Feinberg hypothesis revisited. J Psychiatr Res 28:239–265.

2. Penzes P, Cahill ME, Jones KA, VanLeeuwen J-E, Woolfrey KM (2011): Dendritic spine pathology in neuropsychiatric disorders. Nat Neurosci 14:285–293.
3. Keshavan MS, Giedd J, Lau JYF, Lewis DA, Paus T (2014): Changes in the adolescent brain and the pathophysiology of psychotic disorders. Lancet Psychiatry 1:549–558.
4. Sekar A, Bialas AR, de Rivera H, Davis A, Hammond TR, Kamitaki N, *et al*. (2016): Schizophrenia risk from complex variation of complement component 4. Nature 530:177–183.
5. Arnold SE, Lee VM, Gur RE, Trojanowski JQ (1991): Abnormal expression of two microtubule-associated proteins (MAP2 and MAP5) in specific subfields of the hippocampal formation in schizophrenia. Proc Natl Acad Sci U S A 88:10850–10854.
6. Shelton MA, Newman JT, Gu H, Sampson AR, Fish KN, MacDonald ML, *et al*. (2015): Loss of microtubule-associated protein 2 immunoreactivity linked to dendritic spine loss in schizophrenia. Biol Psychiatry 78:374–385.
7. Rosoklija G, Toomayan G, Ellis SP, Keilp J, Mann JJ, Latov N, *et al*. (2000): Structural abnormalities of subicular dendrites in subjects with schizophrenia and mood disorders: Preliminary findings. Arch Gen Psychiatry 57:349–356.
8. Kalus P, Muller TJ, Zuschratter W, Senitz D (2000): The dendritic architecture of prefrontal pyramidal neurons in schizophrenic patients. Neuroreport 11:3621–3625.
9. Black JE, Kodish IM, Grossman AW, Klintsova AY, Orlovskaya D, Vostrikov V, *et al*. (2004): Pathology of layer V pyramidal neurons in the prefrontal cortex of patients with schizophrenia. Am J Psychiatry 161: 742–744.
10. Garey LJ, Ong WY, Patel TS, Kanani M, Davis A, Mortimer AM, *et al*. (1998): Reduced dendritic spine density on cerebral cortical pyramidal neurons in schizophrenia. J Neurol Neurosurg Psychiatry 65: 446–453.
11. Konopaske GT, Lange N, Coyle JT, Benes FM (2014): Prefrontal cortical dendritic spine pathology in schizophrenia and bipolar disorder. JAMA Psychiatry 71:1323–1331.
12. Bouras C, Kovari E, Hof PR, Riederer BM, Giannakopoulos P (2001): Anterior cingulate cortex pathology in schizophrenia and bipolar disorder. Acta Neuropathol 102:373–379.
13. Moyer CE, Shelton MA, Sweet RA (2015): Dendritic spine alterations in schizophrenia. Neurosci Lett 601:46–53.
14. Kubicki M, McCarley R, Westin CF, Park HJ, Maier S, Kikinis R, *et al*. (2007): A review of diffusion tensor imaging studies in schizophrenia. J Psychiatr Res 41:15–30.
15. Zhang H, Schneider T, Wheeler-Kingshott CA, Alexander DC (2012): NODDI: practical in vivo neurite orientation dispersion and density imaging of the human brain. Neuroimage 61:1000–1016.
16. Jespersen SN, Kroenke CD, Østergaard L, Ackerman JJH, Yablonskiy DA (2007): Modeling dendrite density from magnetic resonance diffusion measurements. Neuroimage 34:1473–1486.
17. Jespersen SN, Bjarkam CR, Nyengaard JR, Chakravarty MM, Hansen B, Vosegaard T, *et al*. (2010): Neurite density from magnetic resonance diffusion measurements at ultrahigh field: comparison with light microscopy and electron microscopy. Neuroimage 49:205–216.
18. Colgan N, Siow B, O'Callaghan JM, Harrison IF, Wells JA, Holmes HE, *et al*. (2016): Application of neurite orientation dispersion and density imaging (NODDI) to a tau pathology model of Alzheimer's disease. Neuroimage 125:739–744.
19. Nazeri A, Chakravarty MM, Rotenberg DJ, Rajji TK, Rathi Y, Michailovich OV, *et al*. (2015): Functional consequences of neurite orientation dispersion and density in humans across the adult lifespan. J Neurosci 35:1753–1762.
20. Glahn DC, Laird AR, Ellison-Wright I, Thelen SM, Robinson JL, Lancaster JL, *et al*. (2008): Meta-analysis of gray matter anomalies in schizophrenia: Application of anatomic likelihood estimation and network analysis. Biol Psychiatry 64:774–781.
21. Francis AN, Mothi SS, Mathew IT, Tandon N, Clementz B, Pearlson GD, *et al*. (2016): Callosal abnormalities across the psychosis dimension: Bipolar schizophrenia network on intermediate phenotypes. Biol Psychiatry 80:627–635.
22. Cannon TD (2015): How schizophrenia develops: Cognitive and brain mechanisms underlying onset of psychosis. Trends Cogn Sci 19:744–756.
23. Hartberg CB, Sundet K, Rimol LM, Haukvik UK, Lange EH, Nesvåg R, *et al*. (2011): Brain cortical thickness and surface area correlates of neurocognitive performance in patients with schizophrenia, bipolar disorder, and healthy adults. J Int Neuropsychol Soc 17: 1080–1093.
24. Cross-Disorder Group of the Psychiatric Genomics Consortium (2013): Genetic relationship between five psychiatric disorders estimated from genome-wide SNPs. Nat Genet 45:984–994.
25. Pearlson GD (2015): Etiologic, phenomenologic, and endophenotypic overlap of schizophrenia and bipolar disorder. Annu Rev Clin Psychol 11:251–281.
26. Ball G, Srinivasan L, Aljabar P, Counsell SJ, Durighel G, Hajnal JV, *et al*. (2013): Development of cortical microstructure in the preterm human brain. Proc Natl Acad Sci U S A 110:9541–9546.
27. Harrison PJ (1999): The neuropathology of schizophrenia: A critical review of the data and their interpretation. Brain 122:593–624.
28. Nuechterlein KH, Green MF, Kern RS, Baade LE, Barch DM, Cohen JD, *et al*. (2008): The MATRICS Consensus Cognitive Battery, part 1: Test selection, reliability, and validity. Am J Psychiatry 165: 203–213.
29. Barch DM, Ceaser A (2012): Cognition in schizophrenia: Core psychological and neural mechanisms. Trends Cogn Sci 16:27–34.
30. Cornblatt BA, Malhotra AK (2001): Impaired attention as an endophenotype for molecular genetic studies of schizophrenia. Am J Med Genet 105:11–15.
31. Knowles EE, David AS, Reichenberg A (2010): Processing speed deficits in schizophrenia: Reexamining the evidence. Am J Psychiatry 167:828–835.
32. Bora E, Yucel M, Pantelis C (2009): Cognitive endophenotypes of bipolar disorder: A meta-analysis of neuropsychological deficits in euthymic patients and their first-degree relatives. J Affect Disord 113: 1–20.
33. Jenkinson M, Beckmann CF, Behrens TEJ, Woolrich MW, Smith SM (2012): FSL. Neuroimage 62:782–790.
34. Smith SM (2002): Fast robust automated brain extraction. Hum Brain Mapp 17:143–155.
35. Avants BB, Tustison NJ, Wu J, Cook PA, Gee JC (2011): An open source multivariate framework for n-tissue segmentation with evaluation on public data. Neuroinformatics 9:381–400.
36. Avants BB, Tustison NJ, Song G, Cook PA, Klein A, Gee JC (2011): A reproducible evaluation of ANTs similarity metric performance in brain image registration. Neuroimage 54:2033–2044.
37. Avants BB, Yushkevich P, Pluta J, Minkoff D, Korczykowski M, Detre J, *et al*. (2010): The optimal template effect in hippocampus studies of diseased populations. Neuroimage 49:2457–2466.
38. Smith SM, Jenkinson M, Johansen-Berg H, Rueckert D, Nichols TE, Mackay CE, *et al*. (2006): Tract-based spatial statistics: Voxelwise analysis of multi-subject diffusion data. Neuroimage 31: 1487–1505.
39. Winkler AM, Ridgway GR, Webster MA, Smith SM, Nichols TE (2014): Permutation inference for the general linear model. Neuroimage 92: 381–397.
40. Smith SM, Nichols TE (2009): Threshold-free cluster enhancement: Addressing problems of smoothing, threshold dependence and localisation in cluster inference. Neuroimage 44:83–98.
41. Lerch JP, Evans AC (2005): Cortical thickness analysis examined through power analysis and a population simulation. Neuroimage 24: 163–173.
42. Robin X, Turck N, Hainard A, Tiberti N, Lisacek F, Sanchez J-C, *et al*. (2011): pROC: An open-source package for R and S+ to analyze and compare ROC curves. BMC Bioinformatics 12:1–8.
43. Klöppel S, Abdulkadir A, Jack CR Jr, Koutsouleris N, Mourão-Miranda J, Vemuri P (2012): Diagnostic neuroimaging across diseases. Neuroimage 61:457–463.
44. Zhang T, Koutsouleris N, Meisenzahl E, Davatzikos C (2015): Heterogeneity of structural brain changes in subtypes of schizophrenia

revealed using magnetic resonance imaging pattern analysis. Schizophr Bull 41:74–84.

45. Chklovskii DB, Schikorski T, Stevens CF (2002): Wiring optimization in cortical circuits. Neuron 34:341–347.
46. Rosoklija G, Keilp JG, Toomayan G, Mancevski B, Haroutunian V, Liu D, *et al*. (2005): Altered subicular MAP2 immunoreactivity in schizophrenia. Prilozi 26:13–34.
47. Rottschy C, Langner R, Dogan I, Reetz K, Laird AR, Schulz JB, *et al*. (2012): Modelling neural correlates of working memory: A coordinate-based meta-analysis. Neuroimage 60:830–846.
48. Minzenberg MJ, Laird AR, Thelen S, Carter CS, Glahn DC (2009): Meta-analysis of 41 functional neuroimaging studies of executive function in schizophrenia. Arch Gen Psychiatry 66:811–822.
49. Cannon TD, Huttunen MO, Lonnqvist J, Tuulio-Henriksson A, Pirkola T, Glahn D, *et al*. (2000): The inheritance of neuropsychological dysfunction in twins discordant for schizophrenia. Am J Hum Genet 67:369–382.
50. Park S, Holzman PS, Goldman-Rakic PS (1995): Spatial working memory deficits in the relatives of schizophrenic patients. Arch Gen Psychiatry 52:821–828.
51. Glahn DC, Therman S, Manninen M, Huttunen M, Kaprio J, Lönnqvist J, *et al*. (2003): Spatial working memory as an endophenotype for schizophrenia. Biol Psychiatry 53:624–626.
52. Saperstein AM, Fuller RL, Avila MT, Adami H, McMahon RP, Thaker GK, *et al*. (2006): Spatial working memory as a cognitive endophenotype of schizophrenia: Assessing risk for pathophysiological dysfunction. Schizophr Bull 32:498–506.
53. Schizophrenia Working Group of the Psychiatric Genomics Consortium (2014): Biological insights from 108 schizophrenia-associated genetic loci. Nature 511:421–427.
54. Pagel T, Baldessarini RJ, Franklin J, Baethge C (2013): Characteristics of patients diagnosed with schizoaffective disorder compared with schizophrenia and bipolar disorder. Bipolar Disord 15: 229–239.